UvA-DARE (Digital Academic Repository)

Inflow and outflow boundary conditions for 2D suspension simulations with the immersed boundary lattice Boltzmann method

Azizi Tarksalooyeh, V.W.; Závodszky, G.; van Rooij, B.J.M.; Hoekstra, A.G.

Inflow and outflow boundary conditions for 2D suspension simulations with the immersed boundary lattice Boltzmann method

Victor W. Azizi Tarksalooyeh [a],*, Gábor Závodszky [a], Britt J. M. van Rooij [a], Alfons G. Hoekstra [a,b]

[a] *Computational Science Lab, Institute of Informatics, University of Amsterdam, The Netherlands*
[b] *ITMO University, Saint-Petersburg, Russian Federation, Russia*

ABSTRACT

In- and outflow boundary conditions for 2D immersed boundary lattice Boltzmann suspension simulations, applied to cell based blood flow models, are presented. The inlet is constructed with an one-way coupling to a periodic domain containing a correct distribution of suspended particles. This provides an inflow of particles that has a correct distribution and is decoupled from any phenomena in the flow domain. An outflow boundary for the particles that does not influence the distribution of particles in the flow domain is also constructed. With this a method to run long (> 1 s) cell based blood flow simulations within any type of domain is provided. These boundary conditions are then used for a simulation of blood flow in a curved vessel with an aneurysm.

1. Introduction

Cell resolved blood flows are studied with various computer models, see e.g. Fedosov et al. [1] or Mountrakis et al. [2]. These models explicitly represent the red blood cells and/or platelets in their model [3] to mimic and explain various effects (e.g. the Fåhræus–Lindqvist effect [4] or thrombus formations [5]). In these studies mostly periodic boundary conditions (PBC) are used for the flow domain. Sometimes, however, it is not possible to use periodic boundaries (e.g. single inlet, multiple outlet flows) and another solution has to be used [6]. In this paper inflow and outflow flow boundaries for complex flows are constructed for suspensions that are modeled with an immersed boundary method [7] on top of a lattice Boltzmann fluid solver [8].

These boundaries are important since the distribution of cells in a blood vessel is non-trivial. This is because of phenomena such as the cell-free layer, Fåhræus–Lindqvist effect or margination of platelets. While periodic boundary conditions might circumvent this problem, they themselves can impose further complications. In a system with PBC the outlet can influence the distribution of particles in the inlet boundary condition (e.g. imagine a thrombus where all platelets get stuck, then this directly causes a depletion of active platelets).

Therefore, we propose another type of inlet and outlet inspired by Lykov et al. [6]. The in- and outlets are decoupled (the outlet cannot influence the inlet) and a separate tubular domain provides a correct distribution of particles and fluid for the inlet boundary condition. Lykov's approach is adjusted for IB-LBM blood suspension simulations. Furthermore Lykov's approach is only validated for very narrow domains (< 10 μm). Our method is also validated for wider domains (∼ 200 μm). A similar approach is proposed by Ye et al. [9]. We extend their method by providing a detailed explanation on how to construct such in- and outlet boundary conditions and how key parameters can be chosen. Finally, we also validate the in- and outlet boundary conditions and show their application in a selected use case.

2. Methods

2.1. Material model for the particles

The material model developed by Mountrakis et al. [10] is used for simulating red blood cells and platelets. This material model is also used for shear experiments [11]. We have tuned this model to increase numerical stability (see Appendix A). The cells are initialized as disks that relax towards their final shape (biconcave for RBCs, platelets stay ellipse shaped) in the first millisecond of a simulation. In a computational context cells are referred to as particles, while the Lagrangian structure points that make up the particles are referred to as lsps.

---

* Corresponding author.
E-mail address: v.w.azizitarksalooyeh@uva.nl (V.W. Azizi Tarksalooyeh).
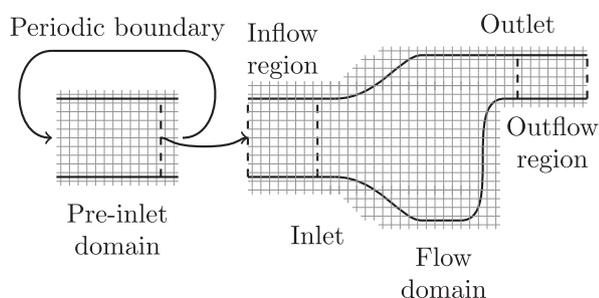
Fig. 1. The various elements necessary for defining the in- and outlet boundary conditions.

Fig. 2. Particle A is transferring into the inflow region. All the lsps of particle A in the inflow region are *ghosts*. Particle B has no more *ghost* particles because it fully entered the inflow region and therefore has been dropped into the fluid. Particle B cannot overlap with particle A because it is repelled from the *ghost* lsps of particle A.

2.2. In- and outflow boundary conditions

A tubular domain with periodic boundary conditions for both the particles and solvent (pre-inlet) is placed in front of the inlet (see Fig. 1). This domain cannot be influenced by the rest of the system in any way. This property implies a one-way communication restriction between the pre-inlet domain and the flow domain. The restriction is enforced by only copying information from the pre-inlet domain to the flow domain. This means that the fluid field and immersed boundary particles must be reconstructed in the flow domain. This is done in the inflow region.

At the end of the flow domain particles have to be removed without influencing the flow domain. This is not possible with a one-way coupling as with the pre-inlet domain and flow domain. Therefore an outflow region is defined in which particles are deleted. The resulting disturbances have no influence on the flow domain before the outlet boundary.

The flow domain is encompassed by the inlet and outlet. Between these boundaries the distribution of particles and fluid is well defined. In the in- and outflow regions the distribution of particles and the fluid flow might not be correct.

It is possible to use different time or space discretisation in the pre-inlet domain because of the one-way communication restriction between the pre-inlet domain and the flow domain. It is even possible to use an entirely different model, as long as the results of that can be interpolated to the inflow region of the flow domain.

2.2.1. Inflow region

At the beginning of the inflow region there is a fluid row which has no neighbors (as it is decoupled from the pre-inlet). This is a classical fluid boundary problem that is well understood for lattice Boltzmann methods [12,13]. We use the macroscopic velocity of a row from the pre-inlet domain to solve the distribution function for this boundary with the method proposed by Zou and He [14]. The immersed boundary method only couples through the macroscopic fluid force and velocity, thus the particles are not affected by the discontinuities in the distribution functions.

The inflow of particles is more intricate. When a lsp of a particle crosses the row from which the macroscopic velocity is copied for the fluid, it is copied to the inflow region. However, all lsps of a particle have to interact to keep the particle in its correct shape. When a particle is transferring from the pre-inlet domain into the inflow region the lsp in the inflow region cannot interact with the lsp in the pre-inlet domain. Therefore, this can cause numerical instability of the particle in the inflow region. Because of this a more complex system for the inlet for particles is proposed.

When a single lsp enters the inflow region it first becomes a *ghost* lsp (see Fig. 2). A *ghost* lsp is used to calculate repulsion for other lsps in the inflow region. This is to ensure no overlap occurs. A *ghost* has no other interaction with lsps and it follows the location of the lsp in the pre-inlet domain it was copied from. To keep
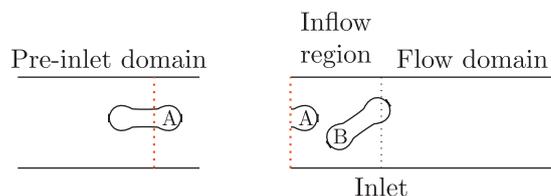
the velocity field of the fluid from deviating from the one in the pre-inlet domain, which would give rise to discontinuities when the particle is finally "dropped into" the inflow region, the force from a *ghost* lsp is communicated through the immersed boundary method to the fluid field in the inflow region as well.

When the full *ghost* particle has crossed the Zou–He boundary at the beginning of the inflow region, all the *ghost* lsps become normal lsps in the inflow region. This happens immediately after the last *ghost* lsp of the *ghost* particle enters the inflow region. This solves the problem of numerical instability of a particle while transferring into the flow domain. The transformation of all *ghost* lsps into normal lsps can be seen as "dropping a particle into the fluid".

The size of the inflow region is dependent on the experiment, but should be at least as long as the length of the longest possible elongated particle in the experiment. With blood flows this is the red blood cell with a maximum length of about 15 µm.

2.2.2. Outflow region

At the end of the outflow region there must be a boundary condition. The same Zou–He boundary as in the inflow region is used, but density is prescribed instead of velocity to calculate the unknown distributions. The density that is used for this is the initial density of the flow domain ρ_0, therefore $\rho_0 = \rho_{\text{out}}$. This boundary condition does not enforce a parabolic profile as expected in a tubular domain. Therefore, a flattening of the velocity profile in the outflow region is to be expected.

A particle is removed fully when one of its lsps crosses the last row of the outflow region (and consequently behavior of the particle becomes undefined). The pressure gradient from the fluid in the particle as opposed to the fluid outside it is approximately zero. Because of this there are no shockwaves resulting of the deletion of a particle. However, the deletion of a particle does influence the particle distribution and flow profile. For this reason the removal is done in the outflow region.

The size of the outflow region is dependent on the experiment and chosen boundary condition. It should be at least as long as the length of the longest possible elongated particle. When the boundary condition introduces artifacts in the outflow region the size of the outflow region should be at least as large to encompass all these artifacts.

2.3. Macroscopic fluid model

The fluid is simulated using the lattice Boltzmann method with the BGK collision operator. The lattice spacing is $\Delta x = 1$ µm. The fluid that is simulated is blood plasma at 37 °C, therefore, the kinematic viscosity is 1.28×10^{-6} m²/s [15,16] and the density is 1025 kg/m³. The timestep is set to $\Delta t = 1.176 \times 10^{-7}$ s. The relaxation time (τ) of the fluid is 1.1. With the particles present this gives an observed locally maximum compressibility error of 1% (as observed from our simulations). This means that the quasi-

Table 1

Dimensions and constants for the pre-inlet plane Poiseuille flow.

Parameter	Value
Diameter, L_d	200 μm
Length, L_p	100 − 500 μm
Hematocrit, H	42 %
Platelet ratio, P	$\frac{1}{20}$
Reynolds number, Re	18
Simulation time, s	1.18 s

Fig. 3. The flow velocity profile of the pre-inlet with aspect ratio 2.5 perpendicular to the flow direction. The black dotted line is the parabolic profile for a fluid flow without particles present in a plane Poiseuille flow with the same average velocity.

Fig. 4. A plot of the hematocrit (solid red line) and platelet concentration (dotted black line) perpendicular to the flow. Fifty samples from five experiments from the largest pre-inlet (500 μm) are used. The samples are taken after a simulation time of 1.0 s. The location of the cell-free layer is plotted on the right.

Fig. 5. A plot of the percentage of marginated platelets for the different pre-inlet domains over time. (For interpretation of the references to color in this figure legend, the reader is referred to the web version of this article)

incompressibility constraint of the lattice Boltzmann method is conserved.

In the pre-inlet domain the fluid is driven by an external forcing term, which is implemented as proposed by Guo et al. [17]. The magnitude of this forcing term is calculated from the Hagen–Poiseuille equation adjusted for flow between parallel plates and a given Reynolds number. In our experiments we choose $Re_{\text{plasma}} = 40$. This results in $\bar{v}_{plasma} = 17$ cm/s for a domain with a width of 200 μm. In our experiments the cells add extra viscosity to the fluid. Since our driving force is constant this results in a lower mean velocity and lower recovered Reynolds number. We measured the resulting mean velocity of the suspension which is $\bar{v}_{susp} = 7.5$ cm/s . Since our flow exhibits laminar behavior we assume that

$$Re_{susp} \approx \frac{\bar{v}_{\text{susp}}}{\bar{v}_{\text{plasma}}} Re_{plasma}$$

which gives us $Re_{susp} \approx 18$. Furthermore this Reynolds number varies slightly with the local hematocrit of the system since the presence of cells in the fluid changes the viscosity.

In the beginning ($t = 0$ s) of a simulation, the body force is increased quadratically from zero to the final magnitude over one millisecond to allow the red blood cells to relax from their initial disk shape to their biconcave shape. A quadratic increase is chosen for numerical stability.
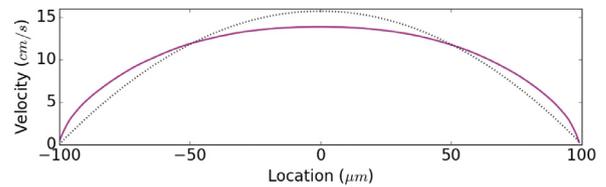
2.3.1. Immersed boundary implementation

The fluid-particle coupling is modeled through an immersed boundary method [7]. In this immersed boundary method the velocity of the fluid is interpolated to the particles at every timestep. The same is true for the force exercised by the material model of the particles on the fluid. This interpolation is done to the closest Eulerian points X with a discrete Dirac delta function as constructed by Mountrakis et al. [10] which effectively gives a four-point stencil with weights to the closest points. No repulsion particles are used at the fluid boundaries.
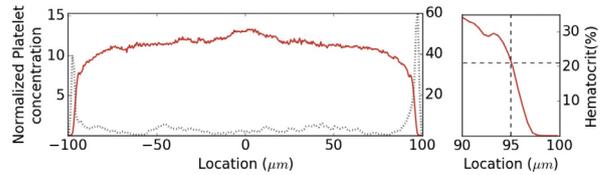
3. Results

3.1. Pre-inlet

Firstly, five differently sized pre-inlet domains are tested to ensure that a correct distribution of particles enters the system. To this end five simulations of each of the five different geometries for the pre-inlet domain are performed. The width of the pre-inlet domain is 200 μm for all geometries ($L_d = 200$ μm). The geometries only differ in length in the direction of the periodic boundary condition (L_p), giving them different aspect ratios defined as the length of a channel divided by its width (L_p/L_d). The aspect ratios range from 0.5 to 2.5 . The rest of the parameters are the same (Table 1).
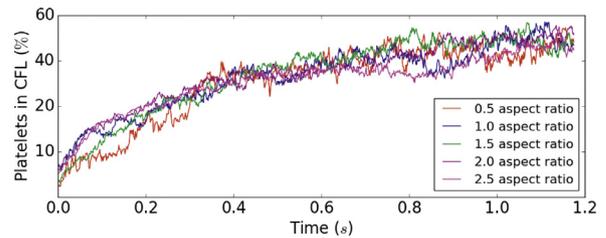
All pre-inlets retrieve similar velocity profiles. Therefore, only the pre-inlet domain with aspect ratio 2.5 is plotted in Fig. 3. Due to the shear thinning behavior of blood the velocity profile is more plug-like than the parabolic profile for a fluid without particle that

has the same average velocity. These finding are supported by Carboni et al. [18].

In flowing whole blood the platelets will marginate to the cell-free layer. This is used as a measure of correctness for the pre-inlets. The margination is measured as the percentage of platelets in the cell-free layer. In relevant literature there is no clear definition of the size of the cell-free layer. Because of this we define it as the maximum length from the wall where there is a hematocrit of at most 50% of the mean hematocrit. This definition for the cell-free layer is used in the rest of this paper. In all the simulations of the pre-inlet domains the cell-free layer is 5 μm according to this definition (see Fig. 4). A platelet is considered marginated when it is present within this layer.

Fig. 5 shows the percentage of marginated platelets over time. The initial margination happens quickly and then asymptotically tends to the final margination percentage, this finding is supported by the work of Pleunis et al. [19] and Zhao et al. [20]. All pre-inlets achieve the same average margination. All pre-inlets seem to recover a correct distribution, however, the system with the largest aspect ratio inherently has the smallest finite size system effects. Therefore we have used the pre-inlet with the largest aspect ratio (2.5) in the following experiment.

3.2. Plane Poiseuille flow

To test the in- and outlet boundary conditions a plane Poiseuille flow is simulated with a pre-inlet domain of the same length as the flow domain (500 μm). See Table 2 for the parameters that are used. At the start ($t = 0$ s) of the simulation only the pre-inlet is filled with particles. The flow domain only consists of fluid. Fig. 6 shows the domain being filled up after turning on the body force

Table 2

Dimensions and constants for the plane Poiseuille flow experiment.

Parameter	Value
Height, d	200 μm
System length, L	500 μm
Pre-inlet length, L_p	500 μm
Hematocrit, H	42%
Platelet ratio, P	$\frac{1}{20}$
Reynolds number, Re	18
Sample step size	0.00118 s
Simulation time	1.18 s
Inflow region	50 μm
Outflow region	50 μm
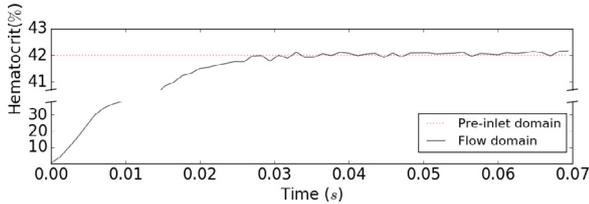
Fig. 6. A plot of the hematocrit over time for the first 0.07 s. The hematocrit is measured and averaged over the full domain (including in- and outflow regions in the flow domain).
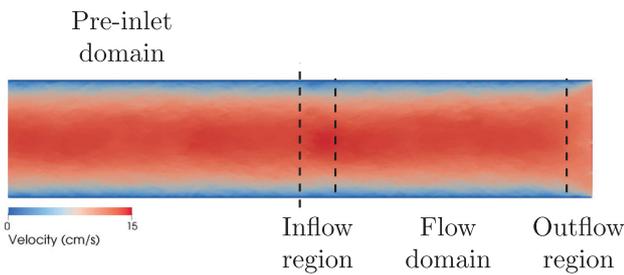

Fig. 7. Velocity magnitude of the fluid in the pre-inlet and the system after 1 s, particles are omitted for visibility.

in the pre-inlet domain. After 0.01 s the flow domain equilibrates around the same hematocrit as the pre-inlet domain.

In Fig. 7 the velocity magnitude of the fluid of the pre-inlet domain coupled with the flow domain is shown. The Zou–He velocity inlet attaches to the pre-inlet with no visible artifacts. At the end of the outflow region the Zou–He density outlet boundary treats all unknown lattice Boltzmann nodes as fluid nodes. Therefore the outlet boundary does not act as an infinite elongation of the plane Poiseuille flow. This results in an more uniform velocity magnitude profile towards the end of the outflow region as expected.

The transformation from the parabolic velocity magnitude profile towards a more uniform profile of the fluid is present in the last 50 μm of the domain. Deviations from the correct particle distributions are not present anymore at that distance from the outlet. Therefore we assume 50 μm to be a large enough outflow region for this simulation.

Fig. 8 shows the pre-inlet domain and flow domain with particles present. The red particles are red blood cells, while the black dots represent the platelets. The graphs on the bottom of Fig. 8 show the averaged hematocrit and platelet concentration for various locations in the flow domain and pre-inlet domain. Through the transition of the pre-inlet domain to the flow domain no noticeable change in this profile is visible. At the end of the outflow region a slight disturbance is visible due to deletion of particles and Zou–He boundary condition artifacts.
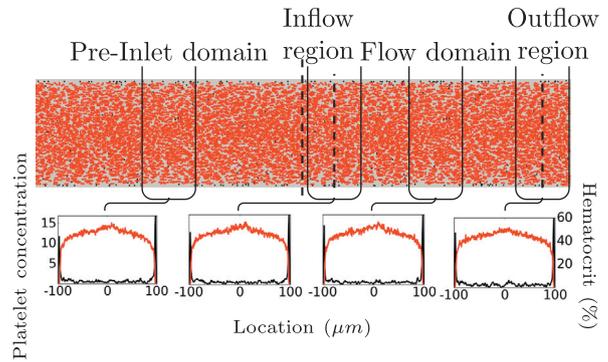
Fig. 8. A comparison of the hematocrit and platelet concentration at different places in the system. The graphs are averaged over 10 samples taken after 1 s of simulation.
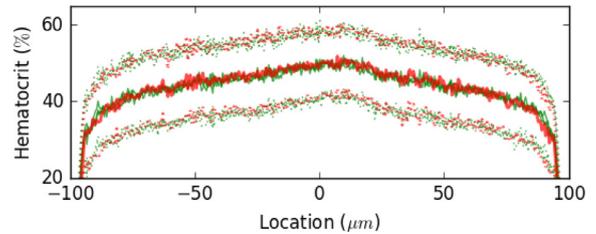
Fig. 9. The profiles from Fig. 8 shown again in a single picture. The solid red line is the hematocrit of the pre-inlet. The solid green lines are the hematocrit of the other three places from Fig. 8. The dotted red and green lines are the standard deviations for these profiles respectively. (For interpretation of the references to color in this figure legend, the reader is referred to the web version of this article.)

### 3.3. Same geometry with pre-inlet and periodic conditions

To show the necessity of our in- and outlet conditions we conduct two experiments with a single geometry. The geometry is such that it can be either run with periodic boundaries or a pre-inlet. The geometry is a straight pipe with diameter of 0.1 cm and an attached aneurysm. We let blood flow through it for 0.4 s with a velocity of 20 cm/s.

In Fig. 10 we can see clear differences arising between the same geometry with different boundary conditions. The aneurysm with pre-inlet is enriched with more platelets than the aneurysm with periodic boundaries. This is due to depletion of platelets in the tube with the periodic conditions. The aneurysm with pre-inlet even has more platelets than are available in the whole periodic system after 0.23 s. Furthermore, the density of particles in the tube with periodic boundary conditions is lower in the aneurysm. We account this effect due to the non-changing number of particles in the whole periodic geometry. Both effects are unwanted and noticeable when running long simulations of such a geometry with periodic boundary conditions. The geometry that is simulated with our new in- and outlet conditions does not suffer from these effects.

3.4. Application to a curved aneurysm

As an example of applying the in- and outlet conditions for an application where periodic boundary conditions cannot be used we simulate the flow of blood within a curved vessel that has an attached aneurysm. Again, the pre-inlet domain that is attached to the curved aneurysm has a width of 200 μm and a length of 500 μm.

The domain is also randomly initialized with the same hematocrit and platelet percentage as the pre-inlet domain. Otherwise the flow domain (aneurysm) would take in the order of seconds to
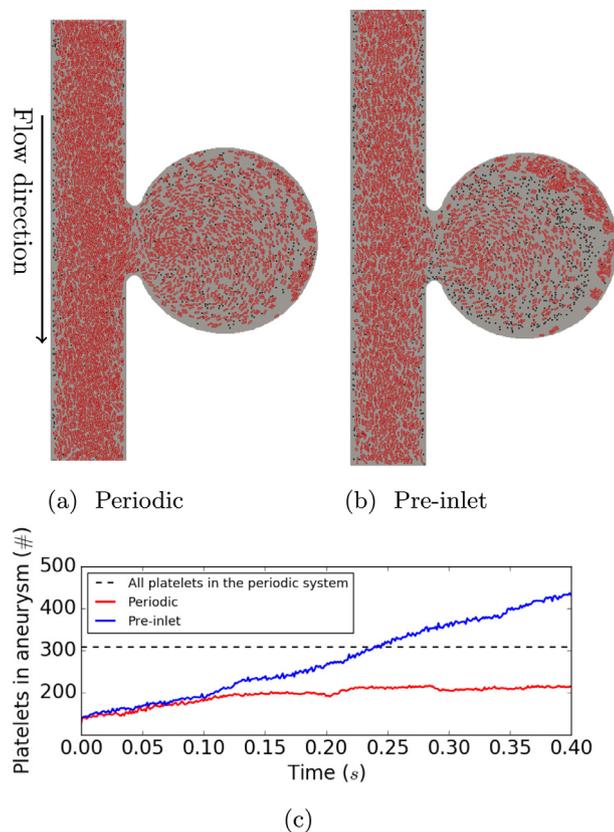
Fig. 10. The same geometry run with periodic (a) and pre-inlet (b) boundaries after 0.4 s. The red cells represent red blood cells and the black cells represent platelets. In (c) the number of platelets in the aneurysm is plotted over time. (For interpretation of the references to color in this figure legend, the reader is referred to the web version of this article.)
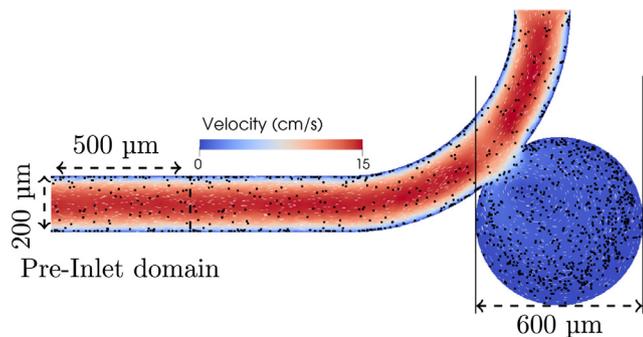
Fig. 11. Curved aneurysm with platelets (black dots), velocity magnitude of the fluid (color bar) and streamlines (white lines). The fluid is moving from the left to the top

reach the correct hematocrit. In the plane Poiseuille flow experiment all these particles would be replaced with particles from the pre-inlet domain within 0.1 s. Thus giving approximately the same simulation results after this time.

Fig. 11 shows the aneurysm after one second of simulation. In this figure the location of a platelet is represented by a black dot. The red blood cells are omitted for clarity. On the background the velocity of the fluid and the streamlines are plotted. We can see that platelets start to accumulate in the aneurysm as predicted by Závodszky et al. [21] and observed in earlier work by Mountrakis et al. in a straight vessel geometry with periodic boundary conditions [22].

4. Discussion and conclusion

We have shown that Lykov's et al. [6] method can be adapted for two dimensional suspensions simulated with IB-LBM. Furthermore, we show that these two dimensional suspensions can scale to larger inflow boundaries of 200 μm. The tests with the plane Poiseuille flow show that an accurate distribution of particles within the flow domain and a well behaving blood flow is retrieved with our in- and outlet boundaries. The simulation with the curved vessel and attached aneurysm demonstrates the importance of such in- and outlet boundary conditions. Since platelets are accumulating in the aneurysm it is necessary to have an inflow that is independent of the behaviour of particles in the system.

These in- and outflow boundary conditions can be extended into three dimensions as a logical next step. As an extension to the curved aneurysm showcase it is possible to do particle residence time analysis [21] and other analyses that were previously only available to pure fluid solvers within hemodynamics. In future work we intend to investigate the behaviour of platelets in aneurysms in more detail, also taking into account the pulsatility of blood flow.

Acknowledgments

Appendix A. Variables and formulae for the material model

The material model used by Mountrakis et al. [10] suffered from instabilities in our simulations. Therefore, some constants and material model equations are adjusted.

In the simulations the red blood cells appeared to be too stiff. This is solved by squaring the angle used in calculating the bending resistance force (f_{trs}). The bending constant C_{trs} is decreased a hundredfold to 1×10^{-9} N/rad.

We noticed numerical instability caused by large forces from the repulsion force ($\mathbf{F}_{rep}$). This seemed to be happening because of a exponential term for the distance. Therefore this term is removed and made linear. This dampens the force impact of collisions that with the quadratic term could create such large forces that the simulation became numerically unstable.

As a final step some parameters for the material model are slightly adjusted (see Table 3).

In the simulations it became apparent that the repulsion force causes the particles to keep a distance of h_{cutoff} from each other at all times. Because of this the particles act as if they have a diameter that is $0.5 \times h_{cutoff} = 0.3$ μm larger. Therefore this extra area is added to the calculation for the hematocrit. This is shown as the apparent area in Table 4.

Table 3
Adjusted constants.

Parameter	Value
Spring constant, C_{spr}	1×10^{-3} N/m
Cell-cell constant, C_{rep}	2×10^{-22} N.m^2
Cutoff distance, h_{cutoff}	0.6 μm

Table 4
Cell properties.

Parameter	Red blood cells	Platelets
Area	$10.00\,\mu m^2$	$1.81\,\mu m^2$
Apparent area	$15.30\,\mu m^2$	–
Circumference	$16.71\,\mu m$	$5.03\,\mu m$
N_{lsp}	26	8

References

[1] Fedosov DA, Dao M, Karniadakis GE, Suresh S. Computational biorheology of human blood flow in health and disease. Ann Biomed Eng 2014;42(2):368–87.

[2] Mountrakis L. Transport of blood cells studied with fully resolved models. Faculty of Science, University of Amsterdam; 2015. Ph.D. thesis.

[3] Moeendarbary E, Ng T, Zangeneh M. Dissipative particle dynamics: introduction, methodology and complex fluid applications a review. Int J Appl Mech 2009;1(04):737–63.

[4] Fåhræus R, Lindqvist T. The viscosity of the blood in narrow capillary tubes. Am J Physiol Leg Content 1931;96(3):562–8.

[5] Tomaiuolo M, Stalker TJ, Welsh JD, Diamond SL, Sinno T, Brass LF. A systems approach to hemostasis: 2. Computational analysis of molecular transport in the thrombus microenvironment. Blood 2014;124(11):1816–23.

[6] Lykov K, Li X, Lei H, Pivkin IV, Karniadakis GE. Inflow/outflow boundary conditions for particle-based blood flow simulations: application to arterial bifurcations and trees. PLoS Comput Biol 2015;11(8):e1004410.

[7] Peskin CS. The immersed boundary method. Acta Numer 2002;11:479–517.

[8] Chen S, Doolen GD. Lattice Boltzmann method for fluid flows. Annu Rev Fluid Mech 1998;30(1):329–64.

[9] Ye SS, Ju M, Kim S. Recovery of cell-free layer and wall shear stress profile symmetry downstream of an arteriolar bifurcation. Microvasc Res 2016;106:14–23.

[10] Mountrakis L, Lorenz E, Hoekstra AG. Validation of an efficient two-dimensional model for dense suspensions of red blood cells. Int J Mod Phys C 2014;25(12):1441005.

[11] Mountrakis L, Lorenz E, Hoekstra A. Scaling of shear-induced diffusion and clustering in a blood-like suspension. EPL (Europhys Lett) 2016;114(1):14002.

[12] Latt J, Chopard B, Malaspinas O, Deville M, Michler A. Straight velocity boundaries in the lattice Boltzmann method. Phy Rev E 2008;77(5):056703.

[13] Succi S. The lattice Boltzmann equation: for fluid dynamics and beyond. Oxford University Press; 2001.

[14] Zou Q, He X. On pressure and velocity boundary conditions for the lattice Boltzmann BGK model. Phys Fluids (1994-present) 1997;9(6):1591–8.

[15] Brust M, Schaefer C, Doerr R, Pan L, Garcia M, Arratia P, et al. Rheology of human blood plasma: viscoelastic versus Newtonian behavior. Phys Rev Lett 2013;110(7):078305.

[16] Peters SA, Woodward M, Rumley A, Tunstall-Pedoe HD, Lowe GD. Plasma and blood viscosity in the prediction of cardiovascular disease and mortality in the Scottish heart health extended cohort study. Eur J Prev Cardiol 2016. 2047487316672004

[17] Guo Z, Zheng C, Shi B. Discrete lattice effects on the forcing term in the lattice Boltzmann method. Phys Rev E 2002;65(4):046308.

[18] Carboni EJ, Bognet BH, Bouchillon GM, Kadilak AL, Shor LM, Ward MD, et al. Direct tracking of particles and quantification of margination in blood flow. Biophys J 2016;111(7):1487–95.

[19] Pleunis Z, Lorenz E, Mountrakis L, Sprik R, van Leeuwen T. Shear-induced transport of platelets in a red blood cell suspension. Pers Commun 2014.

[20] Zhao R, Kameneva MV, Antaki JF. Investigation of platelet margination phenomena at elevated shear stress. Biorheology 2007;44(3):161–77.

[21] Závodszky G, Károlyi G, Szikora I, Paál G. Fractals and chaos in the hemodynamics of intracranial aneurysms. In: The fractal geometry of the brain. Springer; 2016. p. 263–77.

[22] Mountrakis L, Lorenz E, Hoekstra A. Where do the platelets go? a simulation study of fully resolved blood flow through aneurysmal vessels. Interface Focus 2013;3(2):20120089.